Supporting Information

Londono et al. 10.1073/pnas.1321852111

SI Methods

Grooved Plate Formation and Characterization. We assembled a 96-well plate with 48 flat-bottom and 48 grooved-bottom wells. The grooves were sinusoidal in shape, 1 μm in pitch, and 152.7 ± 1.5 nm (SEM) in depth [characterized by atomic force microscopy (AFM), Fig. S1]. Briefly, grooved features were created by replica molding polydimethylsiloxane (PDMS) (Sylgard 184 silicone elastomer kit; Dow Corning Corp.) at a 1:10 ratio of curing agent to base on a silanized holographic diffraction grating film (Edmund Optics). The cured PDMS sheet was then peeled off and used to generate a polyurethane mold from which PDMS replicas were created for assembly into 96-well plates (Fig. S1*A*).

For some guidance propagation experiments assessing grooves parallel to the interface, we created plates in which half the well was flat and the other half of the well was grooved using the procedure outlined in Fig. S1*B*. A piece of diffraction grating film was taped onto a glass slide and spin-coated with Microposit S1811 positive resist (Shipley) for 30 s at 6,100 rpm, resulting in a ∼1.7-μm thin layer of photoresist on the film. The photoresist was soft-baked on a hotplate at 100 °C for 10 min. Subsequently, the film was patterned using UV light with an exposure energy of 155 mJ/cm^2 through a photomask with alternating 9-mm-wide black and blank lines. The photoresist was developed by immersion in MF321 developer (Shipley) for 20 min. Parts that were exposed to UV light washed off, whereas parts that were not exposed stayed on the film covering the grooves and thus creating a flat area. The patterned film was then rinsed with deionized water and dried with nitrogen. The height of the step associated with the interface was quantified using a profilometer (Tencor Alphastep 200; KLA Tencor). PDMS molds were then created from this master as described above. This method led to the presence of a 1-μm groove at the interface between grooved and flat regions, which was not suitable to test the perpendicular propagation case.

To create interfaces without the 1-μm step at the interface, we used the following procedure. A thoroughly cleaned and dried Si wafer was spun-coated first with adhesive primer hexamethyldisilazane (MicroPrime MP- P20 HMDS; Shin-etsu) and then with S1811 positive resist at 4,000 rpm for 40 s. The photoresist was soft-baked at 105 °C for 2 min. Photolithography was done on the resist-coated wafer using a chrome-glass photomask with regions containing 2-μm-pitch lines. The photoresist was exposed to UV light (365 nm wavelength, 16.9 mW/cm^2 intensity) in contact mode for 10 s, using an MA6 Mask Aligner (SUSS MicroTec AG). The unexposed photoresist was removed by MF-321 developer. Dry etching was carried out using inductively coupled plasma reactive ion etcher (Phantom II RIE/ICP System; Trion Technology) at a pressure of 100 mTorr and reactive ion etching rf power of 120 W with SF6, O2, CHF3, and He etchants at 30 sccm, 20 sccm, 12 sccm, and 10 sccm flow rates, respectively, and these settings resulted in an overall etch rate of 400 nm/min. Etching times were adjusted to alter final groove depth and spacing. Before soft lithography, patterned Si wafers (∼630 nm or ∼3.14 μm in depth, characterized by AFM) were washed with acetone and then silanized in a desiccator. Replica molding to obtain grooved substrates was achieved as described above.

Cell Culture and Seeding of Grooved Plates. We conducted experiments using human retinal epithelial (ARPE-19) cells (ATTC) and human foreskin fibroblast (BJ) cells (ATTC). ARPE-19 were grown in DMEM/nutrient F-12 (DMEM/F-12) (Invitrogen) supplemented with 10% (vol/vol) FBS (VWR) and 1% penicillin/streptomycin (VWR). BJ cells were grown in DMEM (ATCC) supplemented with 10% (vol/vol) FBS and 1% penicillin/streptomycin. All cells were maintained in a humidified atmosphere at 37 °C and 5% CO_2. Before seeding, PDMS culture wells were coated with a 10-μg/mL solution of stabilized fibronectin (Biomedical Technologies, Inc.) for 1 h, followed by a PBS rinse. Cells were then seeded at the indicated densities and allowed to attach for 24 h before conducting tracking experiments.

For experiments on wells that were all flat or all grooved, we seeded 22,000 or 65,000 cells/cm^2 in a 96-well plate. Wells in rows A and H and columns 1 and 12 of the plate were filled with 200 μL of PBS and were not used for cell experiments to avoid edge effects arising from temperature or humidity differentials. For experiments using hybrid surfaces containing an interface between flat and grooved regions, we seeded 86,000 cells/cm^2 (for low-density experiments) or 156,000 cells/cm^2 (for all other conditions). These increased seeding densities were necessary to ensure that we generated a confluent sheet with continuous junctions across the interface.

Cell Migration Analysis. Cell tracking was performed using the Multi-Dimensional Motion Analysis application module in the MetaXpress software package (Molecular Devices). This tracking algorithm uses nuclear shape and fluorescent intensity measurements to track the position of individual cells over time, from which cell speed (total travel distance per time), cell velocity (net displacement per time), persistence (velocity per displacement), and angle of migration of each cell could be determined. Median values of speed or velocity were obtained for each well owing to the nonnormal distribution of the data. The mean of all of the well medians from each test condition was then calculated. Coordination of migration between neighboring cells was quantified using a custom-built algorithm [described elsewhere in detail (1)]. Specifically, we calculated the distance over which each cell showed coordinated movement (movement in directions ±10°) with neighboring cells. Based on cell size, stream widths of distances of 40 μm or more represent groups of more than two cells. We quantified, for grooved and nongrooved substrates, the percent of total cells with distances of coordinated movement of 40 μm or greater to obtain the percentage of cells participating in streams. We calculated the average stream width by taking the average stream width of all cells in streams greater than 40 μm in width.

For every well in every experiment, spatial correlation numbers were calculated as a function of distance from each cell and were averaged across all cells across all time intervals (via Eq. **S1** below) (1). The angled brackets signify an average across all cell pairs and time.

$$V(r) = \left\langle \frac{\vec{v_i} \cdot \vec{v_j}}{|\vec{v_i}||\vec{v_j}|} \right\rangle \qquad \textbf{[S1]}$$

In each time interval, the mean velocity calculated from all of the cells was subtracted from each individual cell velocity before calculating the correlation numbers. These correlation numbers were then fit as an exponential and the correlation length was taken to be the inverse of the decay constant.

Guidance Signal Propagation Quantification Method. To quantify the propagation distance in the interface experiments, an algorithm was written in MATLAB to evaluate the alignment of the velocity vectors (calculated at five 1.5-h intervals for each cell) of the moving cells with the groove direction as a function of distance

from the interface. In 40-μm-sized bins, the average velocity of the moving cells in each time interval was calculated for bins up to and including 720 μm from the interface in both the grooved and flat regions. An average velocity vector calculated across all of the time intervals for each bin was then evaluated. By calculating the sine of the velocity angle (cosine in the perpendicular interface experiments), the extent at which the migration of the cells in each bin is in alignment with the groove direction could be determined. Because cells on grooves are constrained to move along the grooves but with no preferred direction, their average velocity cancels out. To avoid this, we squared the sine or cosine values. Because the average value of sine or cosine squared in completely random migration is 0.5 [i.e., $\sin^2(45°)$], we subtracted this value from all calculations to define the value of randomly migrating cells as 0. All of the alignment numbers were then normalized by dividing them by the average alignment of the cells moving on the grooves. By this definition, a value of 1 implies perfect alignment (cells are moving 100% in the groove direction) and 0 implies that cell movement is completely random. The propagation distance was recorded as the binned distance just before the alignment number first became ≤0.321 (value for $\sin^2\theta - 0.5$ at the point where the average cell velocity deviates more than 25°).

Junction and Tension Modifications. Adherens junctions were disrupted by antibody inhibition using modifications to a previously published protocol (2). Specifically, cells were serum-starved for 30 min, after which they were incubated in 4 mM EGTA in serum-free medium. After a PBS wash, 3 μg/mL E-cadherin antibody (clone SHE78-7; Millipore) in serum medium was added to the cells. For control experiments, 3 μg/mL FLAG antibody (Sigma–Aldrich) was added instead. Following 30-min incubation, cell migration experiments were conducted. GFP-N-cadherin–overexpressing cells were produced by transduction of ARPE-19 with a lentivirus containing a GFP-N-cadherin plasmid. Cells were then FACS-sorted for GFP. Levels of N-cadherin staining at the cell membrane were quantified using ImageJ (3). For each image, the fluorescence intensity was measured along the membrane of five cells in 20 spots per cell with the spot size equaling approximately the width of the membrane.

Myosin II activity was decreased with 5 μM of blebbistatin (Sigma–Aldrich), a myosin II ATPase inhibitor, which remained in solution during cell tracking. To increase myosin II activity, cells were treated with 0.25 nM of calyculin A (Cell Signaling Technology) for 30 min before cell tracking experiments. Calyculin A is a type II phosphatase inhibitor that is specific to myosin light-chain phosphatase at low concentrations, thus promoting activation of myosin II.

Immunocytochemistry. Cells were fixed with 4% (vol/vol) paraformaldehyde (Electron Microscopy Sciences) for 10 min and rinsed three times with PBS. The cells were then permeabilized using 0.1% Triton X-100 (Sigma–Aldrich) at room temperature for 20 min. Following permeabilization, cells were stained with rhodamine phalloidin (Invitrogen Life Technologies) for 2 h at room temperature to assess F-actin. To determine microtubule structure, a mouse monoclonal antibody to the β-subunit of tubulin (Abcam) was added at a dilution of 1:1,000 overnight at 4 °C. To image cellular tight junctions in wild-type ARPE-19, a mouse monoclonal antibody to zona occludens-1 (ZO-1) (Invitrogen) was used at a dilution of 1:1,000 overnight. To image N-cadherin, cells were incubated with mouse monoclonal (clone 2G7) N-cadherin antibody (Abcam) at a dilution of 1:100 overnight at 4 °C. After washing three times with PBS for 5 min, all mouse primary antibodies were conjugated with an Alexa 488 anti-mouse secondary antibody (Invitrogen) at a dilution of 1:250 for 45 min at room temperature. To image cellular junctions in mouse antibody-treated cells, cells were fixed in methanol at −20 °C for 15 min and rinsed with PBS three times. Rabbit anti–ZO-1 (Invitrogen) was then applied at room temperature for 3 h, followed by rinsing with PBS three times. An Alexa 488-conjugated secondary anti-rabbit antibody was applied at 1:160 dilution for 2 h at room temperature. Prepared samples were imaged on an Olympus IX-81 inverted laser scanning confocal microscope using a 40×/0.8 LUMPlanFI dipping water objective or an Olympus IX-81 inverted microscope using 32× or 64× magnification.

Modeling Cell Streaming and Signal Guidance Propagation. A numerical model of self-propelled cells was used to study cell interactions across the boundary between grooved and flat domains. The algorithm used in this study is based on a cellular Potts model and has been characterized in detail (4). Cells mechanically interact through an interfacial energy term (encompassing the cell's shear modulus and adhesion) and excluded volume interactions. Cell migration is caused by a propulsive force of constant magnitude on the substrate. The direction of the motile force evolves as a result of a feedback from the cell displacement to the polarity of the cell; such feedback involves a characteristic persistence time. The relative values of the interfacial energy, the motile force, and the persistence time of the cell polarity directly control the emergence of collective behavior. The latter has been quantified in the model in terms of the correlation length of the cell displacements in flat conditions, that is, the typical distance between cells below which their directions of migration are correlated (an alternative measure of stream width). To calibrate the model, we adjusted model parameters to reach particular values of the spatial correlation length. The following parameter values, as defined in ref. 4, produced a correlation length consistent with experimental measurements: surface energy $J = 5$, motile force $\mu = 0.175$, noise $T = 2.5$, and persistence time $\tau = 10$ Monte Carlo time steps.

For our simulations, cells were enclosed in a domain of 74×64 cell diameters in size. Cells located on a strip of width 10 cell diameters on the left side of the domain were biased to move along y, mimicking locally the effects of the grooves on the cells. The grooved domain was periodic in the y direction (i.e., along the interface direction). To test the influence of the correlation length (a measure of stream width) on the signal propagation distance, confluent layers were generated and the value of the motile force was varied keeping all of the other parameters constant. To create either cohesive or noncohesive populations, the surface energy of unbounded cell membrane was set to 5 or 2, respectively. The density of the cell population was controlled in the model by creating homogeneous gaps in the initial cell sheet configuration. To focus on the steady-state dynamics, simulations were run for up to 20,000 Monte Carlo time steps and flow profiles were analyzed between 3,000 and 20,000 time steps and then averaged over time. The propagation distance was measured as the distance between the interface and the position where the mean vertical velocity component (parallel to the interface) falls below 0.5.

Statistics. To test for significant differences between two test groups, we first used an F test to determine whether equal variance could be assumed and then a pooled or nonpooled Student t test to identify significant differences between test groups. To test for the significance of correlation coefficient values, calculated R values from linear regression analysis were compared with critical R values for $n - 1$ degrees of freedom from a table of critical Pearson coefficients. For all tests, P values of less than 0.05 were considered significant.

1. Slater B, Londono C, McGuigan AP (2013) An algorithm to quantify correlated collective cell migration behavior. *Biotechniques* 54(2):87–92.
2. McLachlan RW, Kraemer A, Helwani FM, Kovacs EM, Yap AS (2007) E-cadherin adhesion activates c-Src signaling at cell-cell contacts. *Mol Biol Cell* 18(8):3214–3223.
3. Schneider CA, Rasband WS, Eliceiri KW (2012) NIH Image to ImageJ: 25 years of image analysis. *Nat Methods* 9(7):671–675.
4. Kabla AJ (2012) Collective cell migration: Leadership, invasion and segregation. *J R Soc Interface* 9(77):3268–3278.

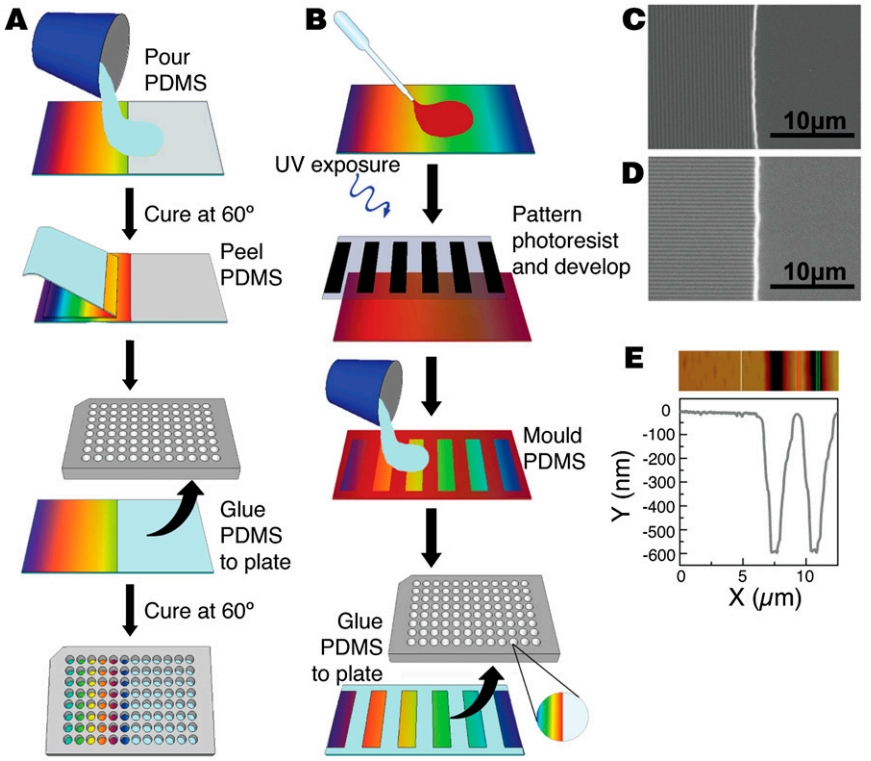

Fig. S1. Fabrication and characterization of a 96-well grooved plate. (*A*) Schematic of method to create completely grooved and flat wells with the plate containing 48 wells of each type. (*B*) Schematic of fabrication approach for a 96-well plate containing wells that are half grooved and half flat. Color gradient indicates grooved regions. (*C* and *D*) Scanning electron micrographs of the grooved–flat interface with the grooves (*C*) parallel and (*D*) perpendicular to the interface. (Scale bars, 10 μm.) (*E*) AFM surface profile of PDMS substrates, showing the interface between flat (left) and grooved (right) sections.

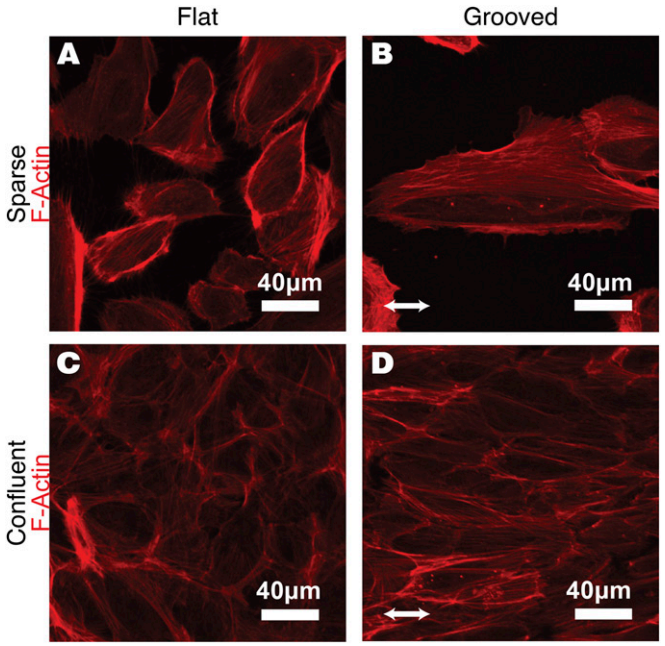

Fig. S2. Alignment of actin in response to grooves. (*A* and *B*) ARPE-19 cells seeded sparsely on grooved and flat PDMS show (*A*) unaligned F-actin on a flat substrate and (*B*) aligned F-actin in the direction of the grooves (white arrow) on a grooved substrate. (*C* and *D*) ARPE-19 cells seeded at confluent densities also show (*C*) unaligned F-actin cytoskeleton on flat PDMS, but (*D*) aligned F-actin on grooves. (All scale bars, 40 μm.)

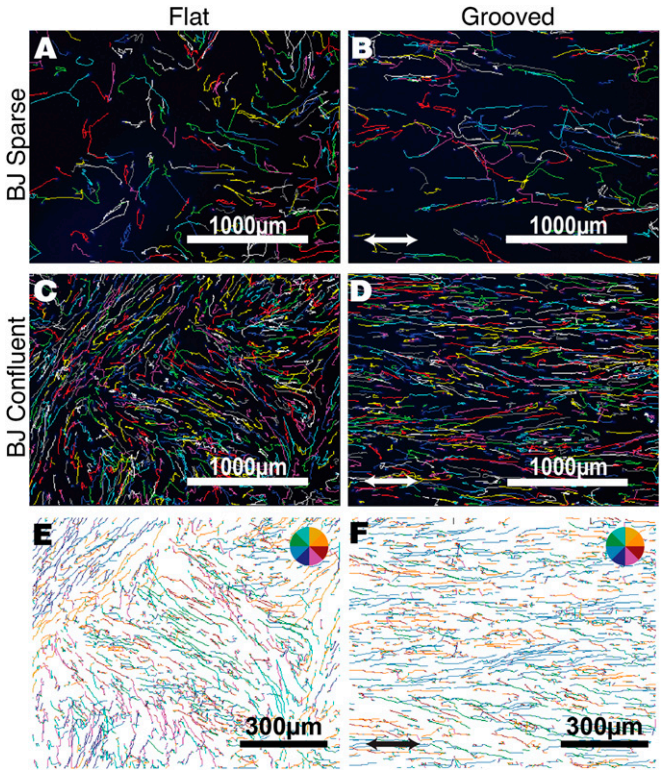

Fig. S3. Imaging and quantification of cell coordination on flat versus grooved substrates. (*A–D*) Representative migration tracks of BJ cells at sparse and confluent cell densities on flat versus grooved substrates. (*A* and *B*) 22,000 BJ cells/cm^2 on (*A*) flat and (*B*) grooved surfaces; (*C* and *D*) 65,000 BJ cells/cm^2 on (*C*) flat and (*D*) grooved surfaces. (*E* and *F*) Cell migration tracks colored by direction of motion to allow easy identification of cellular streams for BJ cells on (*E*) flat and (*F*) grooved substrates. Arrows indicate the direction of grooves in the images. (Scale bars, 1,000 μm for *A–D* and 300 μm for *E* and *F*.)

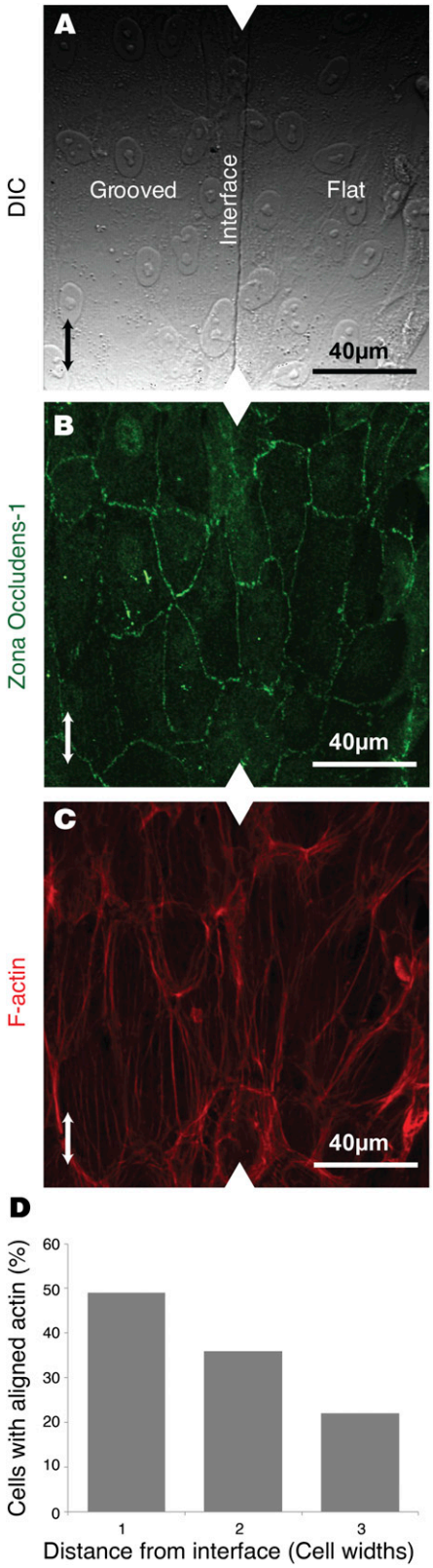

Fig. S4. Assessment of cell sheet formed over grooved–flat interface. (*A*–*C*) Visualization of cell sheet at grooved–flat interface, which is indicated by the arrowheads at top and bottom edges of the images. The direction of the grooves is indicated by the double-headed arrows. (*A*) Differential interference contrast image reveals location of grooved–flat interface, in the center. Cells form a continuous monolayer across the interface as seen through (*B*) the formation of tight junctions and (*C*) the continuity of the actin cytoskeleton. (*D*) Quantification of percentage of cells with F-actin aligned in a direction ±25° of the grooves at different cell distances from the interface. Randomly oriented cells should theoretically show ~27.7% of cells with alignment in the direction of the grooves. Three cells away from the interface (where 22% of cells show aligned actin) the orientation of the actin can therefore be considered random. Quantification was done from 10 images with at least 41 cells analyzed at each distance from the interface. (All scale bars, 40 μm.)

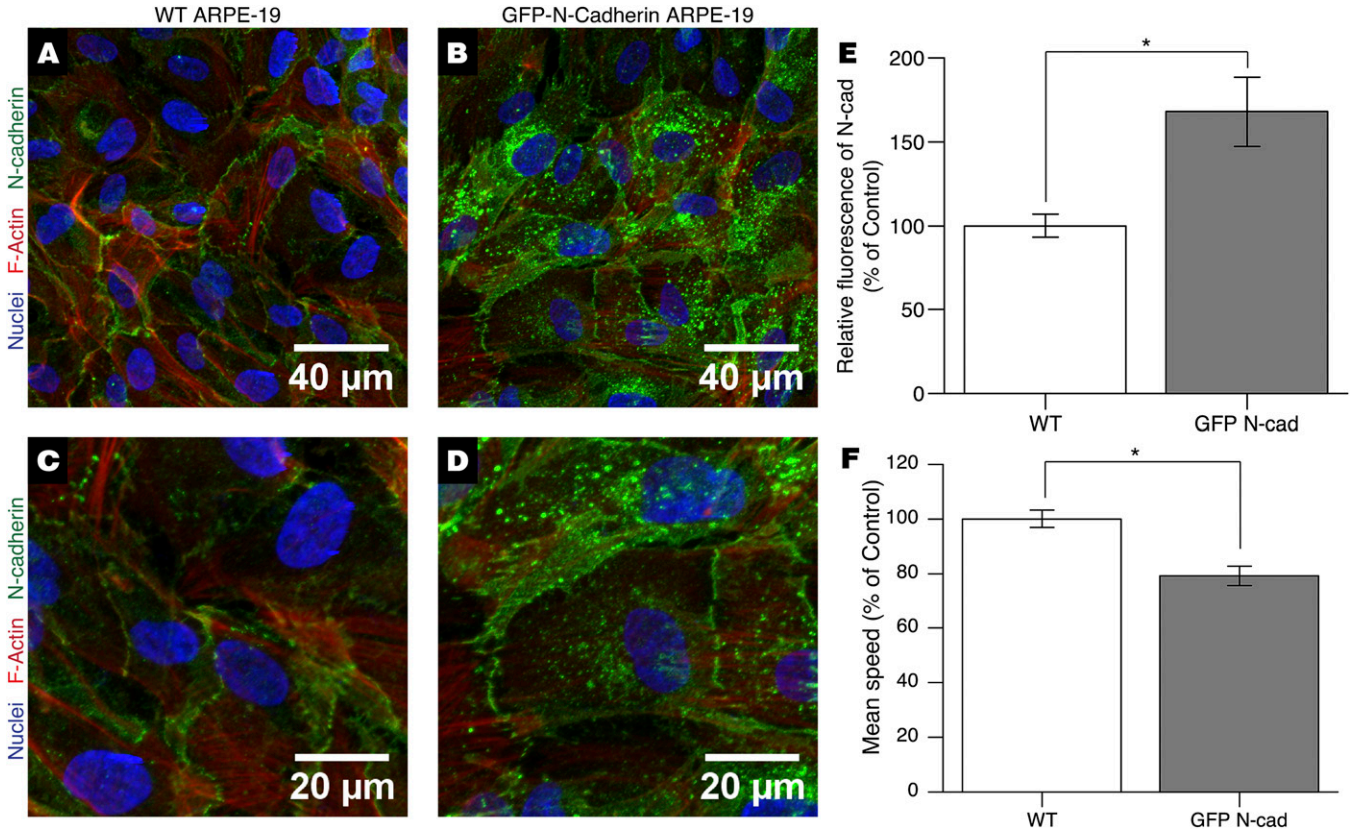

Fig. S5. Characterization of cells expressing GFP-N-cadherin. (*A–D*) Confocal images of N-cadherin (green), nuclei (blue), and F-actin (red) in (*A* and *C*) wild-type cells and (*B* and *D*) N-cadherin–overexpressing cells. (*E*) Quantification of fluorescence levels at cell–cell junctions in wild-type cells and GFP-N-cadherin–overexpressing cells. Significantly higher levels of N-cadherin were present at the cell membranes of GFP-N-cadherin–expressing cells ($P = 7.96 \times 10^{-5}$). (*F*) Impact of N-cadherin overexpression on cell speed. N-cadherin–overexpressing cells (NCad) migrated at significantly slower speeds than wild-type cells ($P = 8.6 \times 10^{-10}$), as expected owing to increased adhesion between the cells. Error bars represent 95% confidence intervals. Arrows indicate the direction and location of grooves in the images. (Scale bars, 40 μm for *A* and *B* and 20 μm for *C* and *D*.)

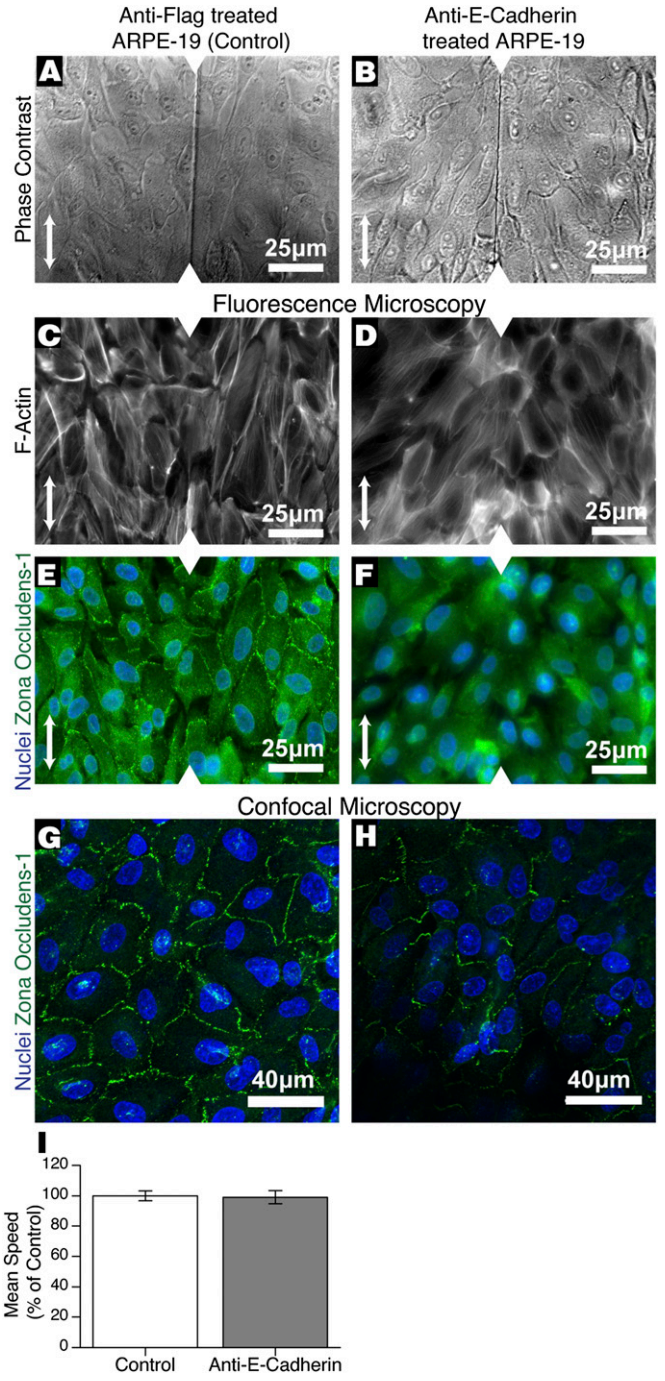

Fig. S6. Characterization of anti–E-cadherin-treated cells. (*A* and *B*) Phase contrast images showing changes in junction contrast on treatment with (*A*) nonspecific anti-FLAG and (*B*) anti–E-cadherin. Spaces between the cells in *B* are more distinct, suggesting junction disruption with the anti–E-cadherin treatment. (*C* and *D*) Actin distribution in cells treated with (*C*) nonspecific anti-FLAG or (*D*) anti–E-cadherin. Peripheral actin is less concentrated in anti–E-cadherin-treated cells consistent with junction disruption. (*E–H*) ZO-1 distribution in cells treated with (*E* and *G*) nonspecific anti-FLAG or (*F* and *H*) anti–E-cadherin. ZO-1 (green), a marker of tight-junction formation, is disrupted in anti–E-cadherin-treated cells consistent with junction disruption. (*I*) Impact of junction strength reduction on cell speed. No significant difference in cell speeds between treated and untreated cells was observed ($P = 0.717$). Double-headed arrows indicate the direction of grooves and arrowheads mark the location of the interface in the images. (Scale bars, 25 μm for *A–F* and 40 μm for *G* and *H*.)

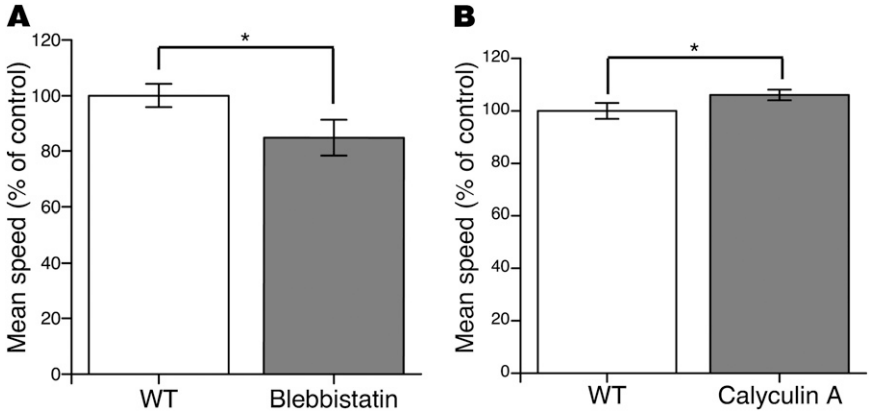

Fig. S7. Characterization of bebbistatin- and calyculin A-treated cells. Mean speed of (*A*) blebbistatin-treated and (*B*) calyculin A-treated ARPE-19 relative to wild-type controls. Blebbistatin treatment significantly reduced cell speed ($P = 1.13 \times 10^{-8}$), whereas calyculin A treatment significantly increased cell speed ($P = 9.94 \times 10^{-4}$). Error bars represent 95% confidence intervals.

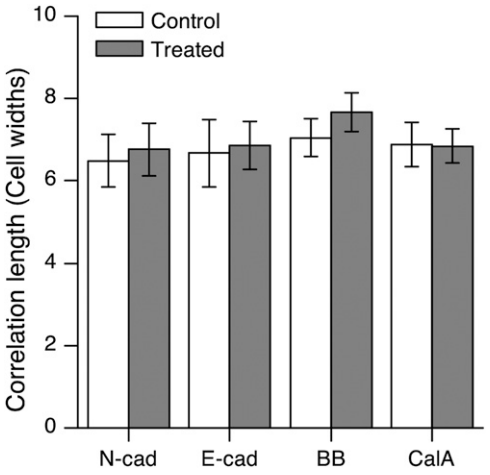

Fig. S8. Correlation lengths in anti–E-cadherin-treated ARPE-19 cells and GFP-N-cadherin–overexpressing ARPE-19 cells, blebbistain (BB)-treated cells and calyculin A (CalA)-treated cells. All measurements were made on cells on flat substrate regions. No significant difference in correlation lengths between treated and control cells was observed ($P = 0.58$ for GFP-N-cadherin, $P = 0.71$ for anti–E-cadherin-treated cells, $P = 0.08$ for BB-treated cells and $P = 0.93$ for CalA-treated cells). Measurements were made on at least 17 wells from at least three independent experiments.

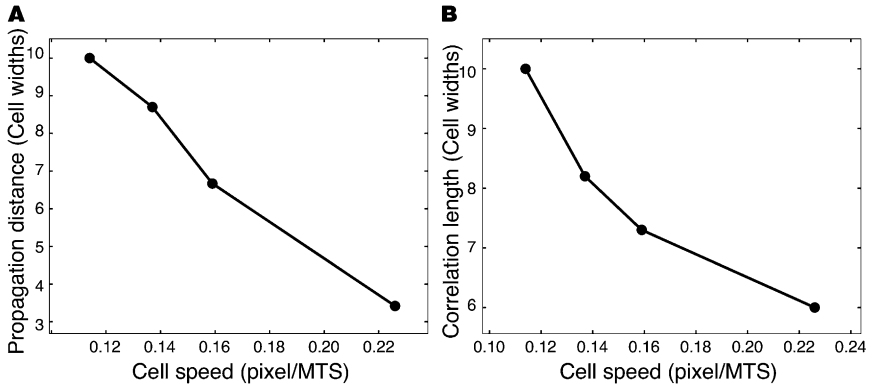

Fig. S9. Assessment of cell speed impact using numerical model. (*A*) Relationship between the propagation distance and the cell speed in the numerical model. (*B*) Correlation length as a function of the cell speed in the numerical model. Cell speed in both cases is calculated in the flat condition from the net displacement over 10 Monte Carlo time steps (MTS) and averaged over 2,300 cells.

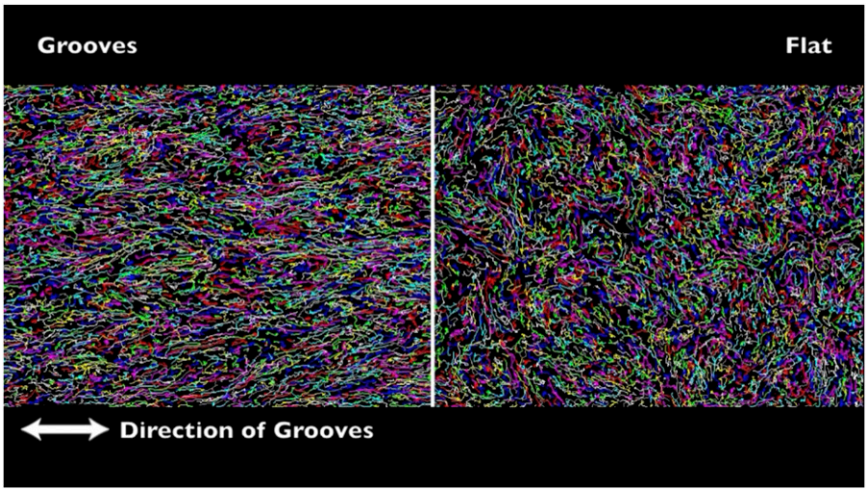

Movie S1. Representative video of ARPE-19 cells migrating within confluent sheets. The right side of the movie shows cells on a flat substrate, and the left side shows cells placed on a grooved substrate. The groove direction is horizontal, as indicated by the double-headed arrow.

Movie S1

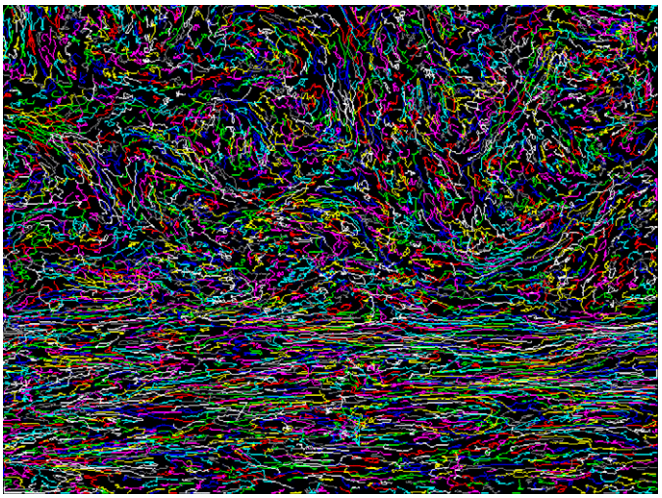

Movie S2. Representative video of ARPE-19 cells migrating within confluent sheets at the interface of hybrid substrates. Grooves are horizontal and located at the bottom portion, and the location of the interface is marked by the arrowheads at the left and right side of the video.

Movie S2

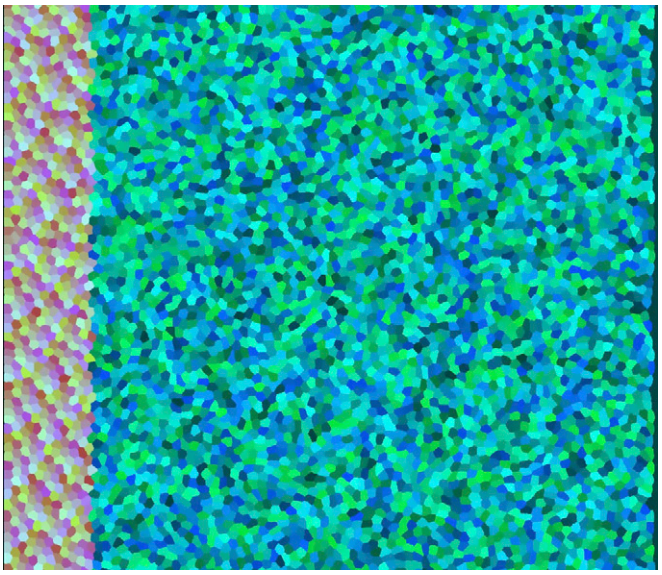

Movie S3. Movie of model simulation of wild-type cell motion on hybrid surfaces. Red/yellow cells are biased to move vertically and mimic cells on the grooves. Green/blue cells have no bias in their behavior and mimic cells on the flat substrate.

Movie S3

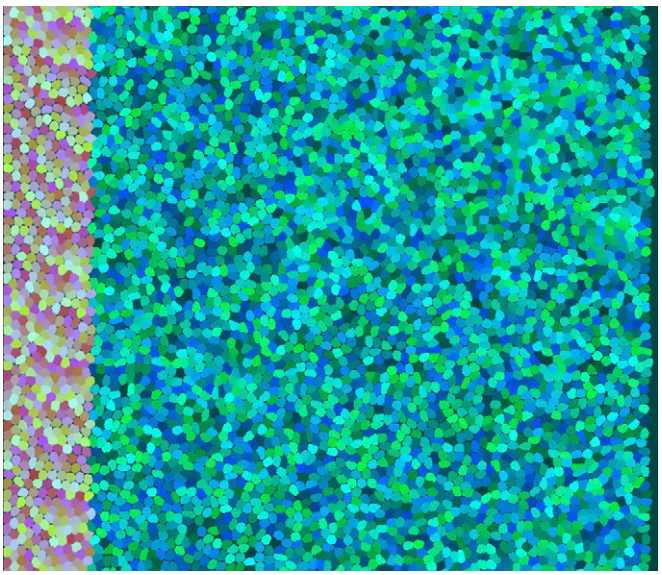

Movie S4. Movie of model simulation of nonadherent cell motion on hybrid surfaces. Red/yellow cells are biased to move vertically to mimic cells on the grooves. Green/blue cells have no bias in their behavior to mimic cells on the flat substrate.

Movie S4